THE JOURNAL OF BIOLOGICAL CHEMISTRY VOL. 282, NO. 33, pp. 24131–24145, August 17, 2007
© 2007 by The American Society for Biochemistry and Molecular Biology, Inc. Printed in the U.S.A.

p62/SQSTM1 Binds Directly to Atg8/LC3 to Facilitate Degradation of Ubiquitinated Protein Aggregates by Autophagy*[S]

Received for publication, April 3, 2007, and in revised form, May 18, 2007 Published, JBC Papers in Press, June 19, 2007, DOI 10.1074/jbc.M702824200

Serhiy Pankiv[‡], Terje Høyvarde Clausen[‡], Trond Lamark[‡], Andreas Brech[§1], Jack-Ansgar Bruun[‡], Heidi Outzen[‡], Aud Øvervatn[‡], Geir Bjørkøy[‡], and Terje Johansen[‡2]

From the [‡]Biochemistry Department, Institute of Medical Biology, University of Tromsø, 9037 Tromsø and the [§]Department of Biochemistry, Institute for Cancer Research, The Norwegian Radium Hospital, Montebello N-0310, Oslo, Norway

Protein degradation by basal constitutive autophagy is important to avoid accumulation of polyubiquitinated protein aggregates and development of neurodegenerative diseases. The polyubiquitin-binding protein p62/SQSTM1 is degraded by autophagy. It is found in cellular inclusion bodies together with polyubiquitinated proteins and in cytosolic protein aggregates that accumulate in various chronic, toxic, and degenerative diseases. Here we show for the first time a direct interaction between p62 and the autophagic effector proteins LC3A and -B and the related γ-aminobutyrate receptor-associated protein and γ-aminobutyrate receptor-associated-like proteins. The binding is mediated by a 22-residue sequence of p62 containing an evolutionarily conserved motif. To monitor the autophagic sequestration of p62- and LC3-positive bodies, we developed a novel pH-sensitive fluorescent tag consisting of a tandem fusion of the red, acid-insensitive mCherry and the acid-sensitive green fluorescent proteins. This approach revealed that p62- and LC3-positive bodies are degraded in autolysosomes. Strikingly, even rather large p62-positive inclusion bodies (2 μm diameter) become degraded by autophagy. The specific interaction between p62 and LC3, requiring the motif we have mapped, is instrumental in mediating autophagic degradation of the p62-positive bodies. We also demonstrate that the previously reported aggresome-like induced structures containing ubiquitinated proteins in cytosolic bodies are dependent on p62 for their formation. In fact, p62 bodies and these structures are indistinguishable. Taken together, our results clearly suggest that p62 is required both for the formation and the degradation of polyubiquitin-containing bodies by autophagy.

All eukaryotic cells use the following two systems for protein degradation: the ubiquitin-proteasome system and the lysosome. The proteasome is used for selective degradation of short lived and abnormal/misfolded proteins following labeling with Lys-48-linked polyubiquitin chains (1). The lysosome degrades extracellular and plasma membrane proteins brought there by endocytosis and cytoplasmic components delivered by autophagy. Various categories of autophagy have been defined differing in the delivery route of cytoplasmic material. These include macroautophagy (hereafter called autophagy), microautophagy, and chaperone-mediated autophagy (2–4). Macroautophagy is regarded as the main pathway. This process involves the sequestration of a region of the cytoplasm within a double or multiple membrane-bounded autophagosome. Autophagosomes then undergo a maturation process, including fusion events with endosomes and/or lysosomes forming structures called amphisomes and autolysosomes, respectively (3–5). Autophagy is thought to be mainly a nonselective, bulk degradation pathway responsible for degradation of the majority of long lived proteins and some organelles. Two evolutionarily conserved protein conjugation systems are necessary for the formation of the autophagosome, the Atg12-Atg5- and the Atg8-phosphatidylethanolamine conjugation systems (6). The best characterized mammalian Atg8 homologue is light chain 3 (LC3).[3] After synthesis pro-LC3 is cleaved by Atg4B to expose a C-terminal glycine residue (7, 8). This represents the cytosolic LC3-I form. Conjugation of phosphatidylethanolamine to the C terminus of LC3-I defines the LC3-II form that is tightly associated with the autophagosomal membrane (7, 9). The LC3-II form is involved during the late steps of autophagy after the isolation membrane has formed (3). In humans, three LC3 isoforms (LC3A, -B, and -C) and four additional human Atg8 homologues have been identified (GABARAP, GEC1/GABARAPL1, GATE16/GABARAPL2, and GABARAPL3) (10, 11). The role(s) of the GABARAP isoforms in autophagy is not known.

A number of studies have identified autophagy as a crucial cellular process to avoid accumulation of abnormal proteins in different neurodegenerative diseases (reviewed in Ref. 12). Mice carrying neuron-specific knock-outs of Atg5 or Atg7 dis-

* This work was supported in part by grants from the FUGE and "Top Research Programme" of the Norwegian Research Council, the Norwegian Cancer Society, the Aakre Foundation, Simon Fougner Hartmanns Familiefond, and the Blix Foundation (to T. J.). The costs of publication of this article were defrayed in part by the payment of page charges. This article must therefore be hereby marked "*advertisement*" in accordance with 18 U.S.C. Section 1734 solely to indicate this fact.

[S] The on-line version of this article (available at http://www.jbc.org) contains supplemental Figs. 1–5.

[1] Recipient of a career fellowship from the FUGE programme of the Norwegian Research Council.

[2] To whom correspondence should be addressed: Dept. of Biochemistry, Institute of Medical Biology, University of Tromsø, 9037 Tromsø, Norway. Tel.: 47-776-44720; Fax: 47-776-45350; E-mail: terjej@fagmed.uit.no.

[3] The abbreviations used are: LC3, light chain 3; ALIS, aggresome-like induced structures; GFP, green fluorescent protein; EGFP, enhanced GFP; mCherry, monomeric red fluorescent protein; GABARAP, γ-aminobutyrate receptor-associated protein; siRNA, small interfering RNA; GST, glutathione *S*-transferase; MBP, maltose-binding protein; LIR, LC3-interacting region; MAP, microtubule-associated protein; MEF, murine embryo fibroblasts; Ab, antibody; mAb, monoclonal antibody.

This is an Open Access article under the CC BY license.

play intracellular accumulation of ubiquitin-positive protein aggregates in the neural cells and show clear symptoms of progressive neurodegeneration (13, 14). By generating mice with a conditional liver-specific knock-out of Atg7, it was also demonstrated that loss of autophagy causes liver dysfunction accompanied by intracellular accumulation of ubiquitinated protein aggregates (15). These results suggest that it is the basal constitutive autophagy that is needed in order to avoid accumulation of ubiquitinated protein aggregates (13, 14, 16).

Recently, the term ALIS (aggresome-like induced structures) was used to describe ubiquitin-containing bodies induced in response to various stressors, including amino acid starvation, oxidative stress, and puromycin (17). ALIS refers to DALIS (dendritic cell aggresome-like induced structures) originally described in lipopolysaccharide-stimulated dendritic cells as storage compartments for polyubiquitinated proteins prior to their degradation (18). ALIS or DALIS are inclusion bodies where newly synthesized ubiquitinated proteins transiently accumulate, many of which are defective ribosomal products (17–19). However, also long lived proteins are targeted to ALIS (17). Puromycin increases the formation of defective ribosomal products and is an efficient inducer of ALIS. ALIS are distinct from aggresomes that are aggregates that form at the pericentriolar area by microtubule-dependent conglomeration of smaller aggregates (20).

The p62 protein, also called sequestosome 1(SQSTM1), is commonly found in inclusion bodies containing polyubiquitinated protein aggregates. In neurodegenerative diseases p62 is detected in ubiquitinated protein aggregates, including Lewy bodies in Parkinson disease, neurofibrillary tangles in Alzheimer disease, and Huntingtin aggregates in Huntington disease (21–24). In protein aggregate diseases of the liver, large amounts of p62 are found in Mallory bodies of alcoholic and nonalcoholic steatohepatitis, hyaline bodies in hepatocellular carcinoma, and in α_1-antitrypsin aggregates (24). The p62 protein is able to polymerize via the N-terminal Phox and Bem1p (PB1) domain (25, 26). It binds ubiquitin and polyubiquitin via its C-terminal UBA domain (27, 28).

Here we report that p62 binds directly to the autophagic effector proteins LC3A and -B and to the related GABARAP and GABARAP-like proteins. A short 22-amino acid region located N-terminally to the UBA domain in p62 was found to be required for this interaction. We developed a novel, pH-sensitive, fluorescent tandem tag, which we use to show that this interaction is necessary for autophagic degradation of p62-positive cytoplasmic inclusion bodies containing ubiquitinated proteins. We also demonstrate that ALIS are indistinguishable from p62 inclusion bodies and that p62 is required for their formation.

EXPERIMENTAL PROCEDURES

Antibodies and Reagents—The following antibodies were used: anti-p62 monoclonal antibody (BD Transduction Laboratories); anti-p62 C-terminal guinea pig polyclonal antibody (Progen Biotechnik); FK2 monoclonal antibody to mono- and polyubiquitinated proteins (Biomol International); anti-GFP antibody (Ab290, Abcam Ltd.); anti-GFP IRDye800-conjugated polyclonal antibody (Rockland Immunochemicals); anti-LC3 monoclonal antibody (NanoTools Antikorpertechnik); anti-actin and anti-LAMP1 monoclonal antibodies (Sigma); and horseradish peroxidase-conjugated anti-mouse and anti-rabbit polyclonal antibody (Pharmingen). The following fluorescent secondary antibodies were used: goat anti-mouse IgG; AlexaFluor 488, AlexaFluor 568, and AlexaFluor 680; goat anti-rabbit IgG AlexaFluor 488; and goat anti-guinea pig AlexaFluor 568 and AlexaFluor 633 (all from Invitrogen). LysoTracker Green and Red and AlexaFluor 647 dextran (M_r 10,000) were obtained from Invitrogen. Bafilomycin A_1 and puromycin were purchased from Sigma. Redivue Pro-mix [^{35}S]methionine was obtained from GE Healthcare.

Plasmids—Plasmids used in this work are listed in Table 1. Details on their construction are available upon request. Point mutants were made using the QuickChange site-directed mutagenesis kit (Stratagene). Gateway LR recombination reactions were done as described in the Gateway cloning technology instruction manual (Invitrogen). Oligonucleotides for mutagenesis, PCR, and DNA sequencing reactions were obtained from Operon. All plasmid constructs were verified by restriction digestion and/or DNA sequencing (BigDye; Applied Biosystems).

Cell Transfections—Subconfluent HeLa cells and mouse embryonic fibroblasts (a generous gift from Noboru Mishizuma) were transfected using Lipofectamine PLUS (Invitrogen). The p62 siRNA SMARTpool oligonucleotide mixture (catalogue number M-010230-00, Dharmacon) or nontargeting siRNAs controls (catalogue number 4635, Ambion; and catalogue number D-001210, Dharmacon) were routinely transfected twice with a 24-h interval at a 20 nM final concentration using Lipofectamine 2000. The specific human p62 siRNA oligonucleotide sequence from the SMARTpool, 5′-GCATTGAAGTTGATATCGAT-3′, was used for most experiments (see supplemental Fig. 1).

Immunoprecipitations and Immunoblots—For immunoprecipitation experiments, cells were lysed 24 or 48 h after transfection in HA buffer (50 mM Tris-HCl, pH 7.5, 150 mM NaCl, 2 mM EDTA, 1 mM EGTA, 1% Triton X-100) with phosphatase inhibitor mixture set II (Calbiochem) and Complete Mini, EDTA-free protease inhibitor mixture (Roche Applied Science). Immunoprecipitations were performed as described previously (29). In Fig. 1 the membrane was stained with Ponceau S, destained, and developed with anti-p62 (BD Transduction Laboratories) followed by AlexaFluor 680-conjugated anti-mouse (Invitrogen) and IRDye800-conjugated anti-GFP (Rockland Immunochemicals) antibodies. The membrane was imaged on an Odyssey infrared imaging system (LI-COR Biosciences).

Mass Spectrometry—Gel bands were excised and subjected to in-gel reduction, alkylation, and tryptic digestion using 2–10 ng/μl trypsin (V511A, Promega) (30). Peptide mixtures containing 0.1% formic acid were loaded onto a nanoAcquity™ Ultra Performance LC (Waters), containing a 3-μm Symmetry® C18 Trap column (180 μm × 22 mm) (Waters) in front of a 3-μm Atlantis™ C18 analytical column (100 μm × 100 mm) (Waters). Peptides were separated with a gradient of 5–95% acetonitrile, 0.1% formic acid, with a flow of 0.4 μl/min eluted to a Q-TOF Ultima Global mass spectrometer (Micromass/Waters) and subjected to data-dependent tandem mass spec-

TABLE 1
Plasmids used in this study

Vectors	*Description*	*Source*
Gateway cloning vectors		
pENTR1A	Entry vector	Invitrogen
pENTR2B	Entry vector	Invitrogen
pENTR3C	Entry vector	Invitrogen
pDest15	Bacterial GST fusion expression vector; T7 promoter	Invitrogen
pDest17	Bacterial 6xHIS fusion expression vector; T7 promoter	Invitrogen
pDEST-TH1	Bacterial MBP fusion expression vector; tac promoter	(54)
pDestEGFP-C1	Mammalian EGFP fusion expression vector; CMV promoter	(25)
pDest-mCherry-C1	Mammalian mCherry fusion expression vector, backbone as pDestEGFP-C1	This study
pDest53	Mammalian GFP fusion expression vector; CMV and T7 promoters	Invitrogen
pDestmyc	Mammalian myc-tag fusion expression vector; CMV and T7 promoters	(25)
pDestGADT7	Yeast two hybrid Gal4 activation domain fusion vector	(25)
pDestGBKT7	Yeast two hybrid Gal4 binding domain fusion vector	(25)
Other vectors		
pEGFP-C1	Mammalian EGFP fusion expression vector; CMV promoter	Clontech
pmCherry-C1	Mammalian mCherry fusion expression vector, backbone as pEGFP-C1	This study
pRSET-B-mCherry	Source of mCherry gene subcloned into mammalian expression vectors	(41)
cDNA constructs made by traditional subcloning or site-directed mutagenesis		
pEGFP-p62	Human p62 in pEGFP-C1 vector	(25)
pGFPC1-LC3	Human LC3B in pEGFP-C1 vector	(55)
pcDNA3-myc-LC3	Human LC3B in pcDNA3-myc vector	(55)
pmCherry-LC3B	LC3B subcloned from pcDNA3-myc-LC3 into pmCherry-C1	This study
pENTR-EGFP	EGFP subcloned from pEGFP-C1 into pENTR1A	This study
pENTR-p62	Human p62 in entry vector	(25)
pENTR-p62K7A/D69A	Human p62 K7A/D69A in entry vector	(25)
pENTR-p62R21A	Human p62 R21A in entry vector	(25)
pENTR-p62(1-385)	Human p62(1-385) in entry vector	(29)
pENTR-p62(124-440)	Human p62(124-440) in entry vector	(29)
pENTR-EGFP-p62	p62 subcloned from pENTR-p62 into pENTR-EGFP	This study
pENTR-EGFP-p62(256-370)	p62(256-370) subcloned from pENTR-p62 into pENTR-EGFP	This study
pENTR-p62$_{SR}$	siRNA resistant p62; codons E254-V255 (gaagtt) mutated to gaggta	This study
pENTR-p62$_{SR}$ ΔLIR	p62$_{SR}$ Δ321-348 in entry vector, made by deletion of pENTR-p62$_{SR}$	This study
pENTR-EGFP-p62$_{SR}$	p62$_{SR}$ subcloned from pENTR-p62$_{SR}$ into pENTR-EGFP	This study
pENTR-EGFP-p62$_{SR}$ ΔLIR	p62$_{SR}$ ΔLIR subcloned from pENTR-p62$_{SR}$ ΔLIR into pENTR-EGFP	This study
pENTR-LC3B	LC3B subcloned from pcDNA3-myc-LC3	This study
pENTR-LC3B(1-28)	LC3B(1-28) subcloned from pcDNA3-myc-LC3	This study
pENTR-LC3B(30-125)	LC3B(30-125) subcloned from pcDNA3-myc-LC3	This study
pENTR-EGFP-LC3B	LC3B subcloned from pcDNA3-myc-LC3 into pENTR-EGFP	This study
pENTR-LC3A	Human LC3A in entry vector, subcloned from image clone 3909192	This study
pENTR-GABARAP	Human GABARAP in entry vector, subcloned from image clone 40022383	This study
pENTR-GABARAP-L1	Human GABARAPL1 in entry vector, subcloned from image clone 5183078	This study
pENTR-GABARAP-L2	Human GABARAPL2 in entry vector, subcloned from image clone 4821535	This study
Other p62 entry vector constructs made by traditional subcloning or site-directed mutagenesis (this study)		
pENTR-p62(124-256)	pENTR-p62(124-385)	pENTR-p62(171-302)
pENTR-p62(231-385)	pENTR-p62(232-370)	pENTR-p62(258-349)
pENTR-p62(281-342)	pENTR-p62(281-328)	pENTR-p62(296-342)
pENTR-p62(321-370)	pENTR-p62(321-349)	pENTR-p62(321-342)
pENTR-p62K7A/D69A(1-385)	pENTR-p62(124-440) Δ303-320	pENTR-p62(124-440) Δ303-349
pENTR-p62K7A/D69A Δ303-349	pENTR-p62K7A/D69A/D335-337A	pENTR-p62K7A/D69A/E323/324A
pENTR-p62K7A/D69A/W338A	pENTR-p62K7A/D69A/E323/324A/D335-337A	
cDNA constructs made by gateway LR reactions (this study)		
pDest15-p62 R21A	pDest15-LC3B	pDest15-LC3A
pDest15-GABARAP	pDest15-GABARAP-L1	pDest15-GABARAP-L2
pDest17-p62K7A/D69A	pDest17-p62K7A/D69A(1-385)	pDest17-p62(124-440)
pDest17-p62(124-385)	pDEST-TH1-p62	pDestmyc-EGFP-p62(256-370)
pDestGADT7-p62(124-385)	pDestGBKT7-LC3B	pDestGBKT7-LC3B(30-125)
pDestEGFP-p62$_{SR}$	pDestEGFP-p62$_{SR}$ ΔLIR	pDest-mCherry-p62
pDest-mCherry-EGFP	pDest-mCherry-EGFP-LC3B	pDest-mCherry-EGFP-p62
pDest-mCherry-EGFP-p62$_{SR}$	pDest-mCherry-EGFP-p62$_{SR}$ ΔLIR	pDest53-p62(124-256)
pDest53-p62(124-440)	pDest53-p62(171-302)	pDest53-p62(231-385)
pDest53-p62(232-370)	pDest53-p62(258-349)	pDest53-p62(281-342)
pDest53-p62(281-328)	pDest53-p62(296-342)	pDest53-p62(321-342)
pDest53-p62(321-349)	pDest53-p62(321-370)	pDest53-p62K7A/D69A
pDest53-p62(124-440)Δ303-349	pDest53-p62(124-440)Δ303-320	pDest53-p62K7A/D69AΔ303-349
pDest53-p62K7A/D69A/D335-337A	pDest53-p62K7A/D69A/E323/324A	pDest53-p62K7A/D69A/W338A
pDest53-LC3A	pDest53-LC3B	pDest53-LC3B(1-28)
pDest53-LC3B(30-125)	pDest53-GABARAP	pDest53-GABARAP-L1
pDest53-GABARAP-L2	pDest53-p62K7A/D69A/E323/324A/D335-337A	

trometry analysis. Peak lists were generated by the ProteinLynx Global server software (version 2.1). The resulting pkl files were searched against the Swiss-Prot 51.6 protein sequence data bases using an in-house Mascot server (Matrix Sciences, London UK). Peptide mass tolerances used in the search were 50 ppm, and fragment mass tolerance was 0.1 Da.

GST- and MBP Pulldown Assays—All GST- and His_6-tagged proteins were expressed in *Escherichia coli* BL21(DE3)pLysS. GST fusion proteins were purified on glutathione-Sepharose 4 Fast Flow beads (Amersham Biosciences). His_6 fusion proteins were purified on Ni^{2+}-nitrilotriacetic acid-agarose columns (Qiagen) and eluted with 0.2 M imidazole, 0.3 M NaCl in phosphate-buffered saline, pH 7.5. MBP fusion proteins were purified on amylose resin (New England Biolabs). ^{35}S-Labeled GFP-tagged proteins were co-transcribed/translated *in vitro* using the TNT T7 coupled reticulocyte lysate system (Promega). For GST pulldowns with His_6-tagged p62 constructs, 2–4 μg of GST-LC3B was incubated with 0.3–0.5 μg of His_6-tagged proteins in 800 μl of NETN-E buffer (50 mM Tris, pH 8.0, 100 mM NaCl, 6 mM EDTA, 6 mM EGTA, 0.5% Nonidet P-40, 1 mM dithiothreitol supplemented with Complete Mini EDTA-free protease inhibitor cocktail (Roche Applied Science)) for 1 h at 4 °C and then washed five times with 1 ml of NETN-E buffer. For GST pulldowns with ^{35}S-labeled GFP-tagged proteins *in vitro*, translation reaction products from 0.5 μg of plasmid were incubated with 1–2 μg of GST-LC3 or LC3 homologues in 300 μl of NETN-E buffer for 1 h at 4 °C, washed six times with 1 ml of NETN-E buffer, boiled with 2× SDS gel loading buffer, and subjected to SDS-PAGE. For GST-pulldowns with ^{35}S-labeled proteins, gels were stained with Coomassie Blue and vacuum-dried. ^{35}S-Labeled proteins were detected on a Fujifilm bio-imaging analyzer BAS-5000 (Fuji). For GST pulldowns with His_6-tagged protein, SDS-PAGE-resolved proteins were transferred to nitrocellulose membrane (Amersham Biosciences) and detected by staining with Ponceau S or immunoblotting with anti-p62 antibody (BD Transduction Laboratories). For MBP pulldowns, 1 μg of MBP or MBP-p62 proteins bound to amylose resin (New England Biolabs) were mixed with 1 μg of GST-LC3B in 200 μl of NETN-E buffer, incubated for 1 h at 4 °C on a rotating wheel, washed six times with 1 ml of NETN-E buffer, boiled with 15 μl of 2× SDS gel loading buffer, and subjected to SDS-PAGE and Western blotting. The nitrocellulose membrane was stained with Ponceau S, followed by immunoblotting with anti-GST antibody.

Confocal Microscopy Analyses—The cell cultures were directly examined under the microscope or fixed in 4% paraformaldehyde and stained as described previously (25). Live cells were placed in Hanks' medium with or without amino acids and serum at 37 °C and imaged for up to 1 h. Images were collected using a Zeiss Axiovert 200 microscope with a ×40, 1.2W C-Apochroma objective, equipped with an LSM510-META confocal module using the LSM 5 software version 3.2 (Carl Zeiss Inc.), or a Leica TCS SP5 confocal microscope, 60×, 1.2W objective, equipped with incubation chamber with CO_2 and temperature control. Images were processed using Canvas version 9 (ACD Systems).

Electron Microscopy—Cells were fixed and embedded as described previously (31). Small blocks were cut and infused

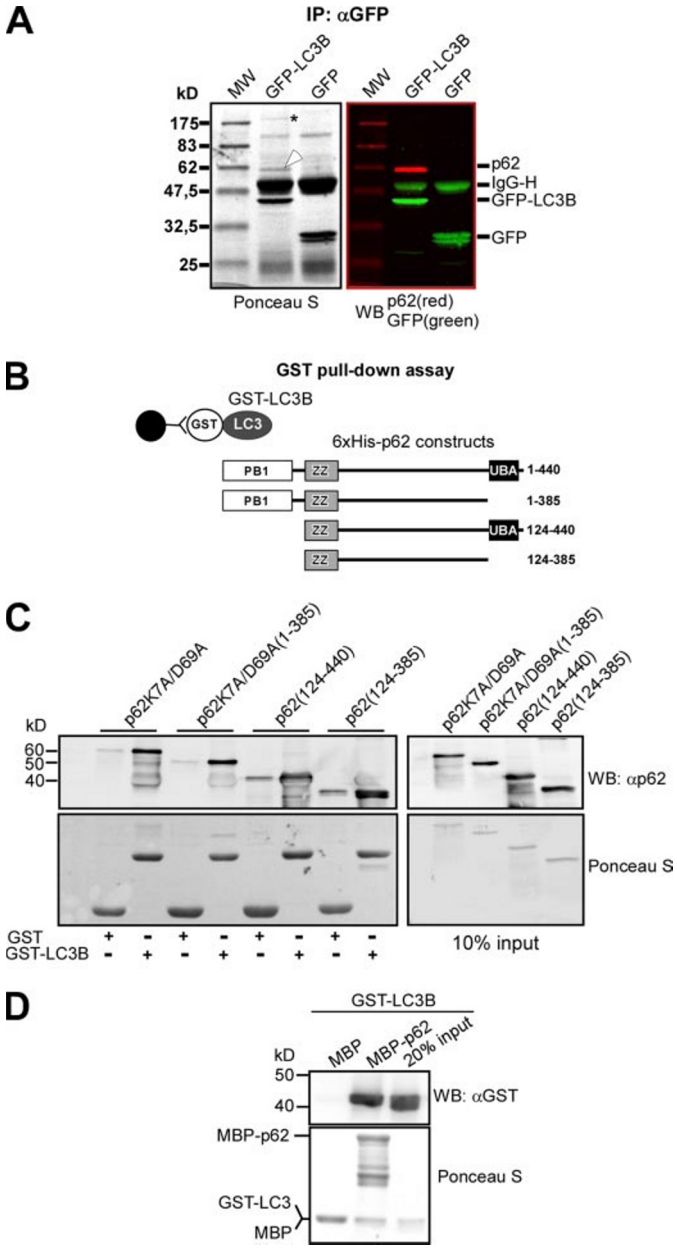

FIGURE 1. **p62 binds directly to LC3B.** *A,* substantial amount of endogenous p62 co-immunoprecipitates with GFP-LC3B from HeLa cell extracts. GFP or GFP-LC3B were immunoprecipitated (*IP*) from total cellular extracts after transiently transfecting the indicated constructs. Co-purified proteins were detected by Ponceau S staining (*left panel*). Using the Odyssey infrared imaging system, endogenous p62 (*red*) was visualized by immunoblotting with anti-p62 antibody, and GFP-LC3B (*green*) was detected using anti-GFP antibody (*right panel*). *WB,* Western blot. The most prominent co-purified protein band was identified as p62 by mass spectrometry (*open arrowhead*). The *asterisk* indicates another prominent band identified by mass spectrometry as MAP1B. *B,* His-tagged p62 constructs used in GST pulldown assays with full-length LC3B. *C,* full-length GST-LC3B binds directly to the central region of recombinant p62. GST-LC3B, purified from *E. coli* and immobilized on glutathione-Sepharose beads, was incubated 60 min with purified, full-length, PB1 or UBA deletion mutants of p62 fused to an N-terminal His_6 tag. After washing the beads five times, bound proteins were eluted by boiling, subjected to SDS-PAGE, and immunoblotted with anti-p62 antibody (*upper panels*) or stained with Ponceau S (*lower panels*). *D,* full-length recombinant p62 fused to MBP binds directly to GST-LC3B. MBP-p62 purified from *E. coli* and immobilized on amylose-resin was incubated with GST-LC3B for 1 h at 4 °C, washed six times, and subjected to SDS-PAGE and Western blotting. The nitrocellulose membrane was stained with Ponceau S followed by immunoblotting with anti-GST antibody.

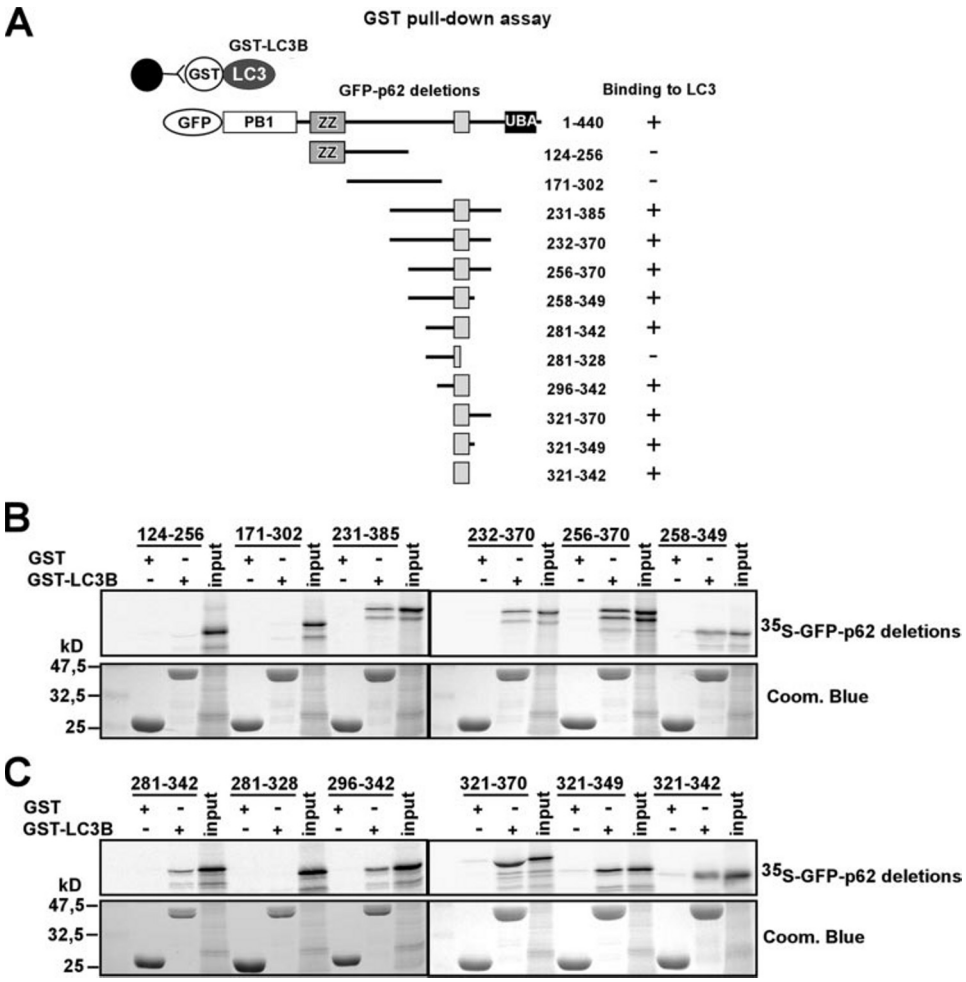

FIGURE 2. **The region spanning amino acids 321–342 of p62 is sufficient for interaction with LC3B.** *A,* constructs used for GST pulldown between full-length LC3B, fused to GST, and deletion mutants of p62. *B* and *C,* mapping of the minimal LIR of p62 by GST pulldown assays between full-length GST-LC3B and deletion mutants of GFP-p62 (or myc-GFP-p62-(256–370)) produced by coupled *in vitro* transcription and translation reaction in the presence of [^{35}S]methionine. Twenty percent of input of proteins translated *in vitro* were run on the same gel. The *upper panels* show the autoradiographs of the gels and the *lower panels* the same gels stained with Coomassie Blue (*Coom. Blue*).

with 2.3 M sucrose for 1 h, mounted on silver pins, and frozen in liquid nitrogen. Ultrathin cryosections were cut at −110 °C on a Leica Ultracut and collected with a 1:1 mixture of 2% methyl cellulose and 2.3 M sucrose. Sections were transferred to Formvar/carbon-coated grids and labeled with primary antibodies followed by protein A-gold conjugates essentially as described (32). After embedding in 2% methyl cellulose, 0.4% uranyl acetate, we observed sections at 60–80 kV in a JEOL 1230 electron microscope. Micrographs were recorded with a Morada digital camera using iTEM (SIS) software. Further image processing was performed using Adobe Photoshop software.

RESULTS

p62/SQSTM1 Binds Directly to LC3—We have shown previously that both endogenous and overexpressed p62 co-immunoprecipitated with GFP-LC3 from HeLa cell extracts (29). However, it is not established if this is because of an indirect or direct protein-protein interaction. It is also not known whether p62 is a major interaction partner for LC3 or not. To begin evaluating the significance of this interaction, we immunoprecipitated GFP-LC3B or GFP from HeLa cells and detected co-immunoprecipitated proteins by staining the membrane with Ponceau S after gel electrophoresis and blotting (Fig. 1*A*, *left panel*). Two bands co-purified specifically with GFP-LC3B as follows: a major 60-kDa band and another larger than the 175-kDa band. The p62 protein was identified in the 60-kDa protein band using a p62 antibody (Fig. 1*A*, *right panel*). To evaluate if the Ponceau S-stained 60-kDa protein band could be a mixture of several proteins, we immunoprecipitated triple FLAG-tagged LC3B, Coomassie-stained the gel after electrophoresis, and excised the 60-kDa band. The gel piece was trypsinized, and eluted peptides were identified by tandem mass spectrometry. Interestingly, the only cellularly derived protein identified in the 60-kDa protein band was p62 (supplemental Fig. 1). To identify the >175-kDa protein, we passed HeLa cell extract over a GST-LC3B column. Bound proteins were eluted and separated by electrophoresis, and the >175-kDa protein band was cut out of the gel and identified as MAP-1B (supplemental Fig. 1). This approach also identified p62 as the major endogenous LC3B-binding protein in the HeLa cell extract. To test whether there is a direct or indirect association between p62 and LC3, we performed pulldown assays with recombinant proteins purified from *Escherichia coli* (Fig. 1, *B–D*). We found a strong binding between GST-LC3B bound to beads and His-tagged p62 (Fig. 1*C*). This was also the case in the reverse experiment where MBP-p62 bound to beads pulled down GST-LC3B (Fig. 1*D*). From the first set of pulldowns the region of p62 binding to LC3B was found to be located somewhere between the N-terminal PB1 domain and the C-terminal UBA domain (Fig. 1*C*). To avoid polymerization of p62 via the PB1 domain, which complicates direct comparison of the binding of full-length, polymeric, and truncated monomeric forms of p62, we used a K7A/D69A mutant of p62 compromising both interaction surfaces of the PB1 domain (25).

Mapping of the LC3 Interacting Region (LIR) of p62—To further map the LC3 interaction region, we made a series of deletion constructs of GFP-tagged p62 that were translated *in vitro* in the presence of [^{35}S]methionine and subjected to GST pulldown experiments with GST-LC3B bound to glutathione-Sepharose beads (Fig. 2). This enabled us to define the region encompassing amino acids 321–342 of human p62 as an LIR.

We could confirm this result by pulldown assays with internal deletions of p62. Deleting amino acids 303–349 in the context of full-length p62 abolished binding to GST-LC3B, whereas deleting amino acids 303–320 did not affect binding of p62 lacking the N-terminal PB1 domain (Fig. 3, *A* and *B*).

The 22-amino acid long LIR is an acidic peptide sequence containing three glutamate and four aspartate residues. We therefore asked if the binding to LC3 could be dependent on electrostatic interactions between acidic residues in LIR and a basic surface of LC3. Because there are acidic residues both in the N- and C-terminal half of LIR, we decided to mutate both clusters separately. Thus, we mutated two consecutive glutamate residues in the N-terminal cluster to alanines (E323A/E324A) and three consecutive aspartate residues in the C-terminal half to alanines (D335A/D336A/D337A) (see Fig. 3*A*). As shown in Fig. 3, *C* and *D*, the binding to GST-LC3B is reduced by 75% upon mutating the C-terminal aspartate residues, whereas it is unaffected by mutating the glutamate residues. As seen from the alignment of p62 sequences from mammals, opossum, chicken, frogs, fishes, sea urchin, and honeybee, it is apparent that the most conserved motif is D(D/E) (D/E)WT at the C-terminal end of LIR (Fig. 3*A*). This is consistent with our finding that mutation of the DDD motif strongly affects binding to LC3. We also found that a single alanine substitution of the absolutely conserved Trp-338 residue had the same dramatic effect as mutating the DDD motif, whereas similar substitutions of the conserved Thr-339 residue and the serines at 332 and 342 had no effect (Fig. 3*A* and data not shown).

Both a crystal structure of form I of rat LC3B and a solution structure of human form I LC3B have been reported (33, 34). The LC3-I structure consists of an N-terminal subdomain (residues 1–29) with two α-helices and a C-terminal subdo-

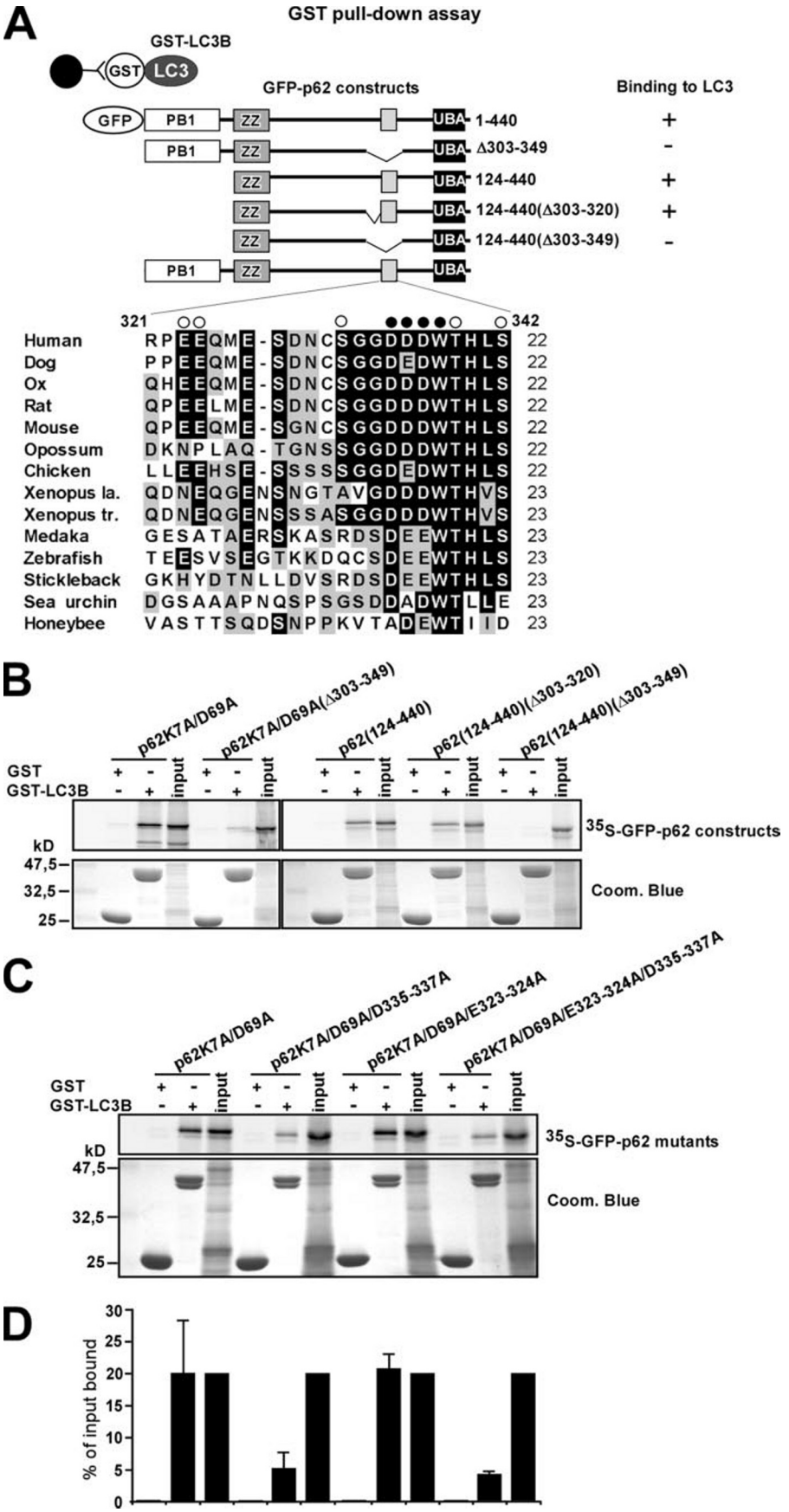

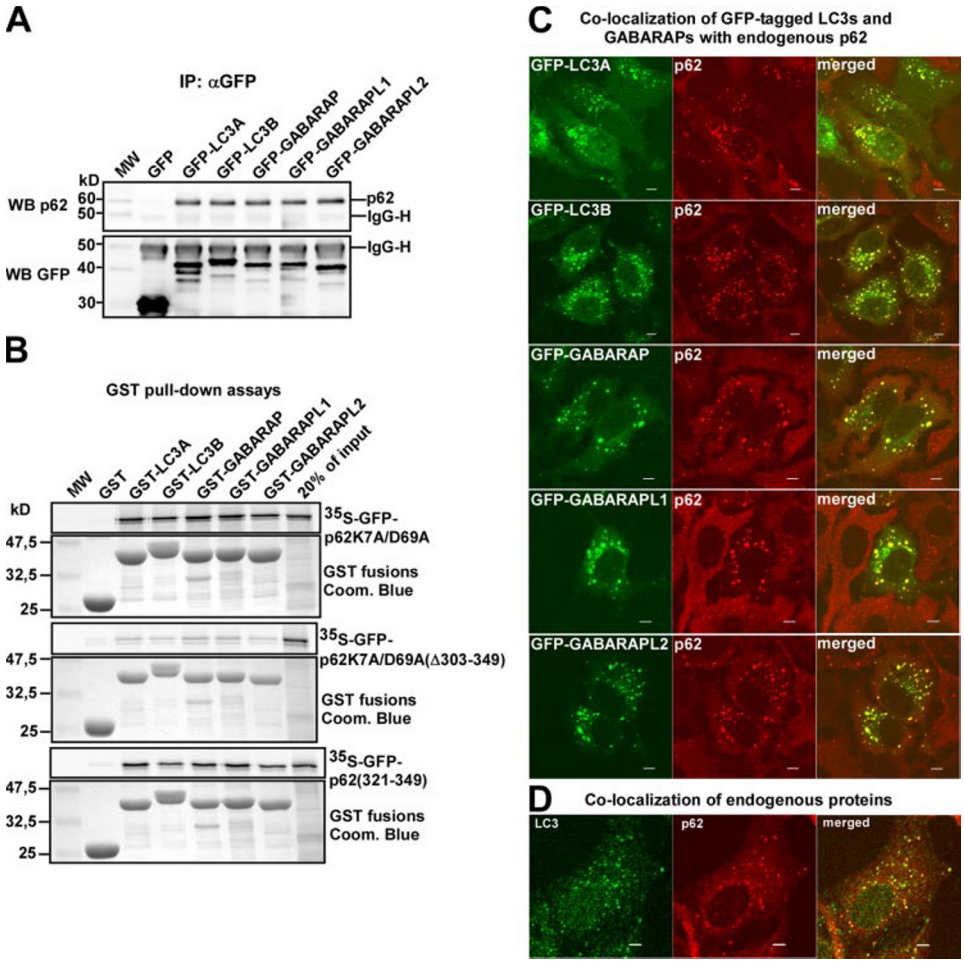

FIGURE 4. **p62 interacts with other MAP1LC3 family proteins.** *A,* endogenous p62 co-immunoprecipitates with GFP fusions of LC3A, LC3B, GABARAP, GABARAPL1, and GABARAPL2 from HeLa cell extracts. GFP or GFP fusion constructs of LC3 family proteins were immunoprecipitated (*IP*) from total cellular extract of transfected HeLa cells and subjected to SDS-PAGE. Co-purified p62 was detected by immunoblotting with anti-p62 antibody (*upper panel*). *WB,* Western blot. Immunoprecipitated GFP fusion proteins were detected with an anti-GFP antibody (*lower panel*). *B,* direct interaction between p62 and LC3 family members was assessed using GST pulldown assays as described in the legend to Fig. 2*B*. *Coom. Blue,* Coomassie Blue. *C,* GFP fusion proteins of LC3A, LC3B, GABARAP, GABARAPL1, and GABARAPL2 co-localize with endogenous p62 (visualized with anti-p62 antibody staining) after transient transfection in HeLa cells. *D,* endogenous LC3 and p62 co-localize in cytoplasmic bodies. HeLa cells were fixed and immunostained with p62 Ab and LC3 mAb. *Scale bars* are 5 μm.

main (residues 30–120) that adopt a ubiquitin fold. Surprisingly, neither the N-terminal subdomain (residues 1–28) nor the C-terminal subdomain of human LC3B interacted with p62 in GST pulldown assays, whereas full-length LC3B bound strongly to p62 (data not shown). Consistent with the results from the pulldown experiments, only full-length LC3B interacted with the central part of p62 in the yeast two-hybrid system (data not shown).

p62 Binds Both to LC3A and -B and the Related GABARAP Family Proteins—LC3B is only one of several homologues of yeast Atg8 found in mammals, including the GABARAP family of proteins (35). We therefore wanted to determine whether p62 could bind to other Atg8 homologues. To this end we transiently expressed GFP-tagged LC3A, LC3B, GABARAP, GABARAPL1, and GABARAPL2 in HeLa cells and subjected cell extracts to immunoprecipitation using an anti-GFP antibody. Co-immunoprecipitation of endogenous p62 was then assessed by immunoblotting with a monoclonal anti-p62 antibody. As shown in Fig. 4*A*, endogenous p62 was co-immunoprecipitated at the same efficiency with GFP-tagged LC3A, GABARAP, GABARAPL1, and GABARAPL2 as with LC3B. Next, we performed GST pulldown assays where we incubated GST-tagged LC3- and GABARAP family proteins, purified from *E. coli* and immobilized on glutathione-Sepharose beads, with three different *in vitro* translated, ^{35}S-labeled GFP-p62 constructs. As shown in the *top panel* of Fig. 4*B*, full-length p62 as represented by GFP-p62K7A/D69A bound strongly to all LC3 and GABARAP proteins tested. If the LIR found to bind to LC3B is deleted, as in the GFP-p62K7A/D69A(Δ303–349) construct tested in the *middle panel* of Fig. 4*B*, the interactions were abolished. However, the LIR alone is sufficient for binding to all GST-tagged LC3- and GABARAP family proteins (Fig. 4*B*, *lower panel*).

Our finding of a direct interaction between p62 and the human Atg8 homologues tested here prompted the question whether these proteins would localize to p62 bodies upon transient overexpression in cells. To test this HeLa cells were transfected with the different GFP-tagged LC3 and GABARAP proteins, and the cells were fixed and stained for endogenous p62. Confocal fluorescence microscopy demonstrated a striking co-localization of these GFP fusion proteins to p62 bodies (Fig. 4*C*). Taken together, our results show that p62 is able to bind in a similar manner to all the five tested Atg8 human homologues and that these proteins can localize to p62 bodies in cells. Using an antibody raised against an N-terminal peptide of LC3B, we were also for the first time able to clearly

FIGURE 3. **Characterization of the LIR of p62 by deletion mapping and point mutations.** *A,* summary of GST pulldown assays between full-length LC3B fused to GST and deletion mutants of p62 (*upper panel*). The *lower panel* shows an alignment of the LIR of human p62 to the corresponding sequences of representatives of mammals, birds, frogs, fishes, sea urchins, and insect species. A triple alanine substitution of the DDD motif and a single alanine substitution of the conserved Trp residue strongly inhibited binding as indicated by *filled circles* above the alignment. *Open circles* indicate alanine substitutions without effect. *B,* interaction between GST-LC3B and *in vitro* translated, ^{35}S-labeled deletion mutants of GFP-p62 analyzed by GST pulldown assays. *C,* p62 residues Asp-335 to Asp-337 are required for efficient interaction with LC3B. *D,* quantitation of the GST pulldown assays as shown in *C*. The data are the mean ± S.D. from three independent experiments. *Coom. Blue,* Coomassie Blue.

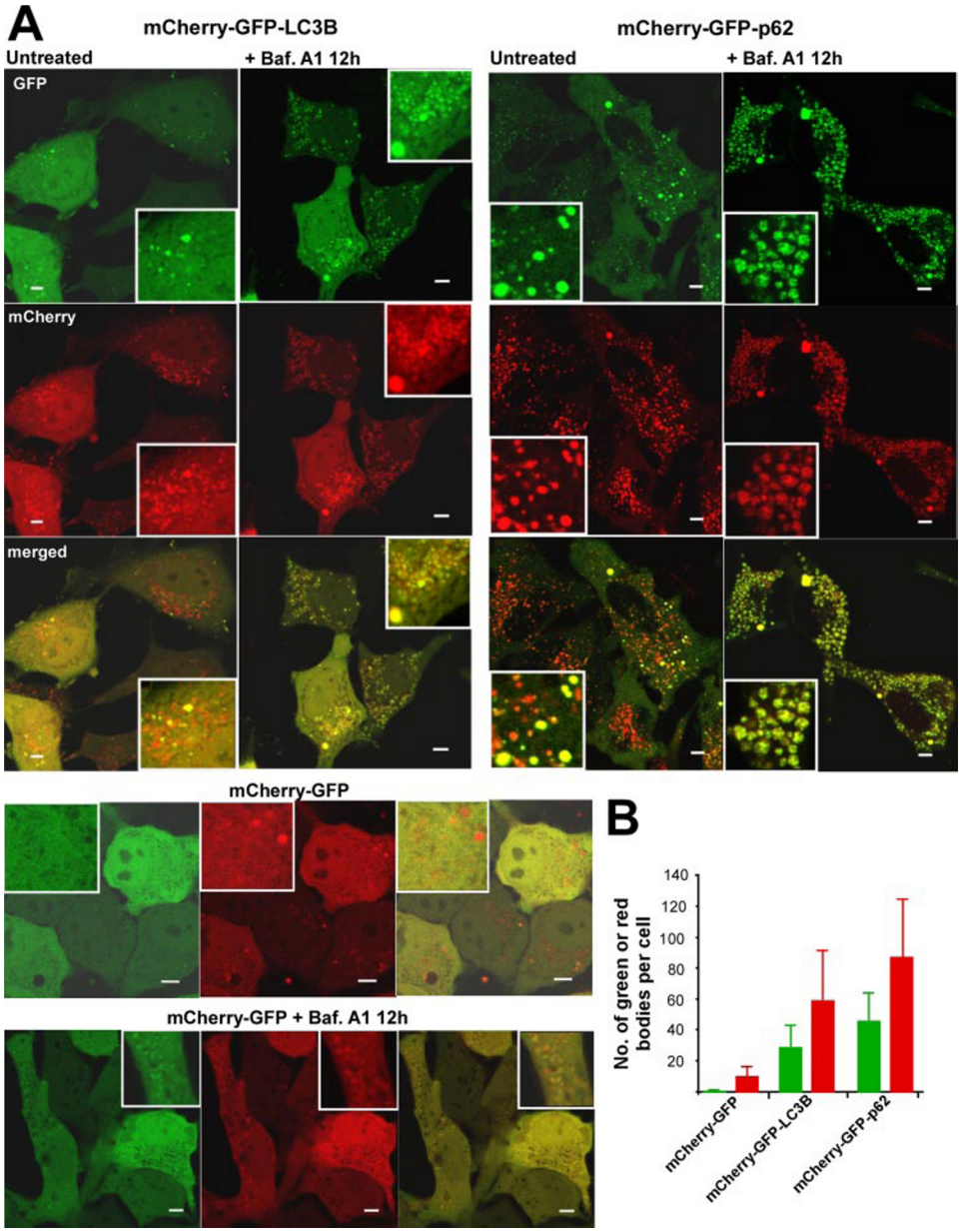

FIGURE 5. **Due to the acid-stable mCherry protein the double tag strategy enables live cell imaging of proteins within acidic vesicles not identified with GFP.** *A,* HeLa cells were transfected with mCherry-GFP-p62, mCherry-GFP-LC3B, or mCherry-GFP. Cells were left untreated or bafilomycin A_1 (*Baf. A1*) (0.2 μM) was added for 12 h. *B,* graphic presentation of the average number of fluorescent structures present per cell 48 h after transfection. The number of fluorescent bodies per cell in 50 cells was counted for each data point shown (each bar). *Scale bars* are 5 μm.

demonstrate co-localization of endogenous LC3 with p62 in cytoplasmic bodies (Fig. 4*D*).

A Novel Double Tag Strategy Makes It Possible to Visualize LC3 and p62 in Acidic Autophagic Vesicles in Live Cells—p62 forms cytoplasmic aggregates that contain polyubiquitinated proteins and LC3 (29). GFP-LC3 is being widely used as a marker of autophagosomes (36, 37). A drawback is, however, that EGFP is acid-labile with a pK_a of 6.0 (38). This makes it difficult to use GFP fusions to follow autophagosomes by fluorescence microscopy after they become acidified following fusion with endosomes or lysosomes to produce amphisomes or autolysosomes. The pH of the lumen of early endosomes may vary from pH 6.1 to 5.5, and late endosomes usually have a pH of about 5.5 and lysosomes have a pH of about 4.7 (39, 40). Another point is that GFP-LC3 will, due to its direct interaction with p62, also localize to p62-positive inclusion bodies making it impossible to use fluorescence microscopy to distinguish between autophagosomes and nonmembrane-confined p62 bodies. To alleviate these problems we fused the monomeric red fluorescent protein mCherry to LC3B. The pK_a of mCherry is $<$4.5, making the protein very acid-stable (38, 41). By exchanging EGFP with the acid-stable mCherry fluorescent tag, we were able to visualize autophagic intermediates not identified with EGFP. Initial co-transfections of p62 containing single EGFP- and mCherry tags clearly demonstrated that all green structures were red and revealed a high number of red structures that were not green (data not shown). However, in co-transfections it is often difficult to obtain the same expression level of the different co-expressed proteins in individual cells. We therefore devised a mCherry-GFP double tag strategy to further improve the ability to distinguish neutral p62 inclusion bodies and autophagosomes from acidic amphisomes and autolysosomes. By expressing mCherry-GFP-LC3B in HeLa cells, we were able to visualize LC3B in acidic vesicles of homogeneous size (0.3–0.6 μm) displaying red fluorescence only, and in neutral structures of more variable size displaying both green and red fluorescence (Fig. 5). Counting of fluorescent structures in live cells revealed that about half of the visible structures were acidic (red only). We counted an average of about 60 red dots and 30 green dots per cell (Fig. 5*B*). Western blot analyses confirmed the expression of double-tagged fusion proteins of correct size (supplemental Fig. 2). Bafilomycin A_1 is an inhibitor of the vacuolar ATPase that blocks acidification of the lysosomes and thereby also lysosomal degradation without affecting the fusion of autophagosomes with lysosomes (42). This way autophagosomes accumulate within lysosomes. In cells treated with bafilomycin A_1, LC3B was found in neutral vesicles, most with a size very close to that of the acidic dots in untreated cells (0.4–0.8 μm) (Fig. 5). Most of these structures are presumably neutralized autolysosomes. To verify that also p62 is present in acidic vesicles, mCherry-GFP-p62 was

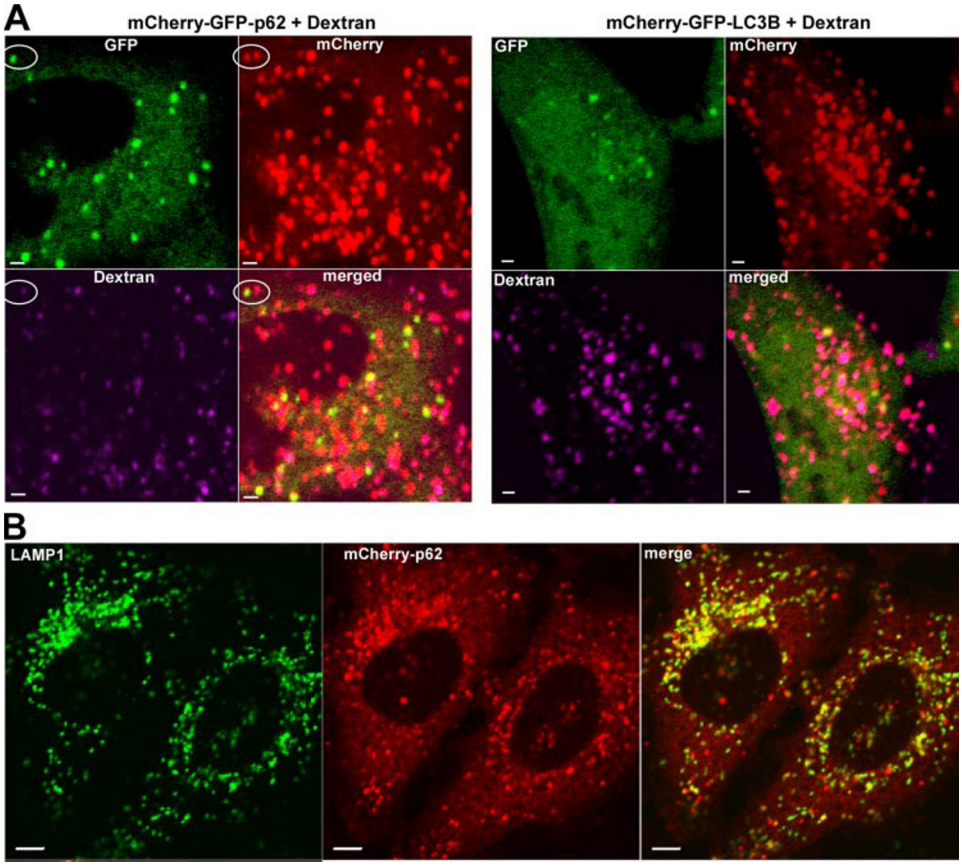

FIGURE 6. **The mCherry-GFP double tag makes it possible to distinguish acidic autophagic vesicles from neutral p62-positive inclusion bodies/autophagosomes.** *A,* in HeLa cells expressing mCherry-GFP-p62 or -LC3B, GFP-positive inclusion bodies, and autophagosomes are not labeled with dextran (*pink*), whereas GFP-negative structures are efficiently labeled with dextran (amphisomes and autolysosomes). An example of two such different structures alongside each other is *encircled*. HeLa cells were incubated with AlexaFluor 647 dextran (*pink*) for 2 h. *B,* co-localization of LAMP1 and mCherry-p62 in HeLa cells. LAMP1 was visualized following permeabilization with 40 μg/ml digitonin using a monoclonal LAMP1 antibody and an AlexaFluor 488-coupled secondary antibody (*green*). *Scale bars* are 5 μm.

expressed in HeLa cells. As expected, p62 was found in both acidic and neutral structures. The acidic vesicles, amounting to half (about 40 per cell) of the fluorescent structures, generally had a size very similar to those formed by LC3B (around 0.5 μm). However, larger acidic structures were also seen. The neutral (yellow) structures vary in size and mobility and represent a mixture of p62-positive inclusion bodies and autophagosomes (29) (Fig. 5). Treatment with bafilomycin A_1 strongly increased the number of neutral structures, very similar to what was observed with mCherry-GFP-LC3B (Fig. 5). To compare the results obtained with p62 and LC3B with those of a randomly degraded protein, we expressed the double tag itself. When expressed in HeLa cells, relatively few weak signals of mCherry-GFP could be detected in acidic vesicles of untreated cells and in neutral structures after treatment of cells with bafilomycin A_1 (Fig. 5). However, the difference between the double tag alone and the double tag fused to either LC3B or p62 is striking and strongly supports the notion that LC3B and p62 are specifically recruited into autophagosomal structures.

To verify that the acidic structures visualized with mCherry-GFP-p62 or mCherry-GFP-LC3B were due to fusions between autophagosomes and endosomes/lysosomes, we looked for co-localization with the endocytic pathway marker AlexaFluor 647 dextran (M_r 10,000). Strikingly, only the red acidic structures co-localized with dextran, whereas the green and red (yellow) structures did not (Fig. 6*A* and supplemental Fig. 3). CD63 is often used as a marker for late endosomes/lysosomes and is highly enriched in multivesicular endosomes (43). In co-transfection experiments we also found strong co-localization between mCherry-LC3B or mCherry-p62 and GFP-CD63 highly suggestive of an amphisomal localization (data not shown). Furthermore, in most cells expressing mCherry-LC3 or mCherry-p62, there was a significant co-localization of mCherry-positive structures with the lysosomal marker LAMP1 (Fig. 6*B*). In similar experiments with cells expressing GFP-LC3 or GFP-p62, no co-localization with LAMP1 was seen (data not shown).

To further confirm that the double tag approach faithfully reports autophagic activity, we expressed mCherry-GFP-p62 in $Atg5^{-/-}$ murine embryo fibroblasts (MEFs) and in m5-7 cells (44, 45). The latter cell line represents $Atg5^{-/-}$ MEFs containing an Atg5 Tet-Off allele enabling autophagic acitivity to be turned off by adding doxycycline to the growth medium. As seen from Fig. 7, in $Atg5^{-/-}$ MEFs mCherry-GFP-p62 is visualized as both green and red fluorescent signals both in inclusion bodies and in a considerable diffuse fraction in the cytoplasm. As expected, the $Atg5^{-/-}$ MEFs were completely unable to recruit mCherry-GFP-p62 into acidic vesicles (Fig. 7 and data not shown). This was also the case in the majority of m5-7 cells when autophagy was turned off in the presence of doxycycline. Some of the cells recruited p62 into acidic vesicles, but this is presumably because of residual expression of Atg5 from the Tet-regulated allele. In contrast, in m5-7 cells where Atg5 expression is turned on, allowing autophagy to occur, there is a large fraction of acidic (red only) p62-containing vesicles indicative of amphisomes and autolysosomes. Based on the counting of fluorescent structures in more than 100 cells, the average number of acidic structures per cell increased from 4 to 25% in response to the induction of Atg5 expression. Taken together, all these results confirm the notion that the red vesicles observed with p62 or LC3B labeled with the double tag most likely represent amphisomes and autolysosomes.

p62-positive Cytoplasmic Bodies Are Degraded by Autophagy—From the above experiments it is not evident whether it is the diffuse fraction of p62 or the p62-positive inclusion bodies

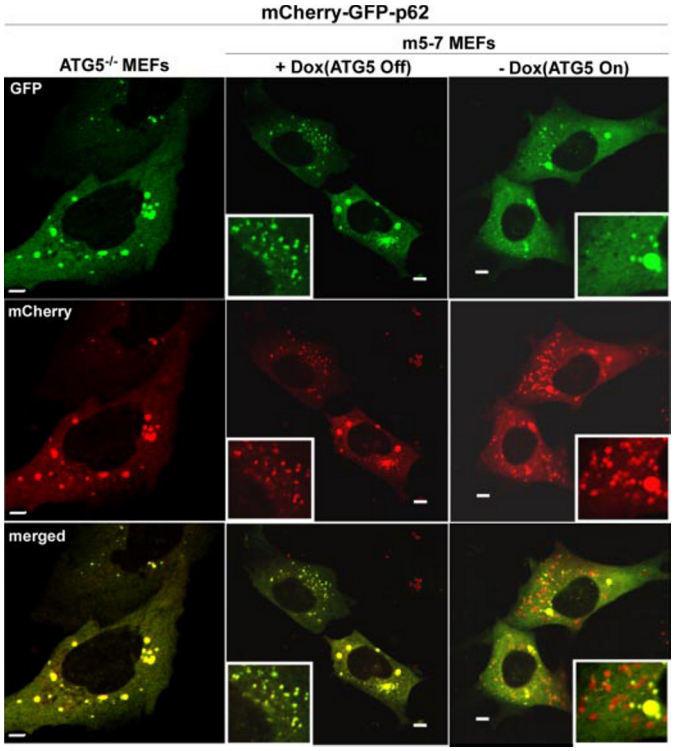

FIGURE 7. **Acidification of p62 bodies containing mCherry-GFP-p62 is dependent on autophagy.** ATG5$^{-/-}$ MEFs were transfected with mCherry-GFP-p62 and live cells imaged 48 h after transfection (*left panel*). Double-tagged mCherry-GFP-p62 was expressed in ATG5$^{-/-}$ MEFs containing a Tet-Off-regulated Atg5 allele (m5-7). Doxycycline (*Dox*) (5 ng/ml) (*middle panel*) was added for 3 days to turn off Atg5 expression or cells were left untreated to allow Atg5 expression and autophagy to occur (*right panel*). *Scale bars* are 5 μm.

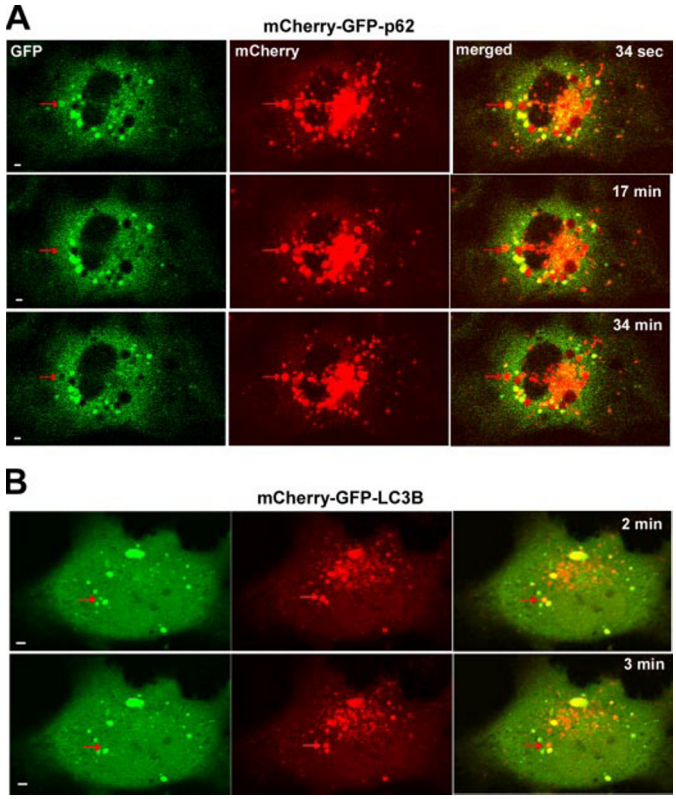

FIGURE 8. **Acidification of large p62-positive bodies visualized with mCherry-GFP-p62 and mCherry-GFP-LC3B.** HeLa cells were transiently transfected with mCherry-GFP-p62 (*A*) or mCherry-GFP-LC3B (*B*). At 48 h after transfection cells were imaged with a Zeiss LSM510 META confocal microscope at a single focal plane, with a pinhole opened to 300 μm to compensate for out-of-plane movements of mCherry-GFP-p62 or mCherry-GFP-LC3B structures. *Scale bars* are 2 μm.

that are specifically degraded by autophagy. It is problematic to make a clear functional distinction between p62 bodies and diffuse p62, because the latter fraction of p62 may include polymeric structures that interact with ubiquitinated proteins and LC3. Using mCherry-GFP-LC3B or mCherry-GFP-p62 for live cell imaging in the confocal fluorescence microscope, we were able to follow p62 bodies through the acidification step most likely occurring upon fusion of autophagosomes with late endosomes and/or lysosomes. Interestingly, we observed that even rather large p62 bodies are clearly degraded by autophagy. Shown in Fig. 8*A* is a series of still images obtained by video confocal microscopy of HeLa cells expressing mCherry-GFP-p62. These images illustrate the acidification of a large p62 body (2 μm in diameter), observed as the loss of green fluorescence whereas the red fluorescence is retained. Similarly, the acidification of a double tag-labeled LC3B dot is shown in Fig. 8*B*. To look for p62-positive inclusion bodies within autophagosomal structures by immunoelectron microscopy, HeLa cells transiently expressing GFP-p62 were treated with bafilomycin A_1 to increase the number of amphisomes/autolysosomes. We observed GFP-p62 localization in cytosolic, membrane-free structures of varying size (supplemental Fig. 4*A*) and in various membrane-enclosed compartments. We recognized electron-dense areas containing GFP-p62 both within typical autophagosomes (supplemental Fig. 4*B*) and within amphisomes/autolysosomes (supplemental Fig. 4, *C* and *D*). The size of these structures varied, but in general they corresponded well with the size of acidic mCherry-GFP-p62 dots observed by confocal imaging. Together, the EM and live cell imaging data strongly suggest that also large p62 bodies can be degraded by autophagy.

p62 Is Required for the Formation of ALIS—The formation of polyubiquitin-positive inclusion bodies is an inducible feature of various cell types (17, 18). Puromycin is commonly used to increase the production of truncated and misfolded proteins, and it dramatically increases the formation of large cytosolic bodies containing misfolded and polyubiquitinated proteins (17, 19). This process has been most studied with dendritic cells, but similar structures are also formed in other cells such as HeLa (17). We therefore asked if inclusions induced by puromycin are actually p62 bodies, and whether p62 has an architectural role in the formation of such structures. The level of endogenous p62 protein can efficiently be reduced by transfection with siRNA (29). Three of four SmartPool siRNAs (Dharmacon) were effective against human p62. Transfection with one of these siRNAs gave efficient knockdown of endogenous p62 even at 5 nM (supplemental Fig. 5). Interestingly, we found that puromycin-induced bodies contain p62, and a dramatic reduction in their number was observed following siRNA-mediated knockdown of p62 (Fig. 9, *A* and *B*).

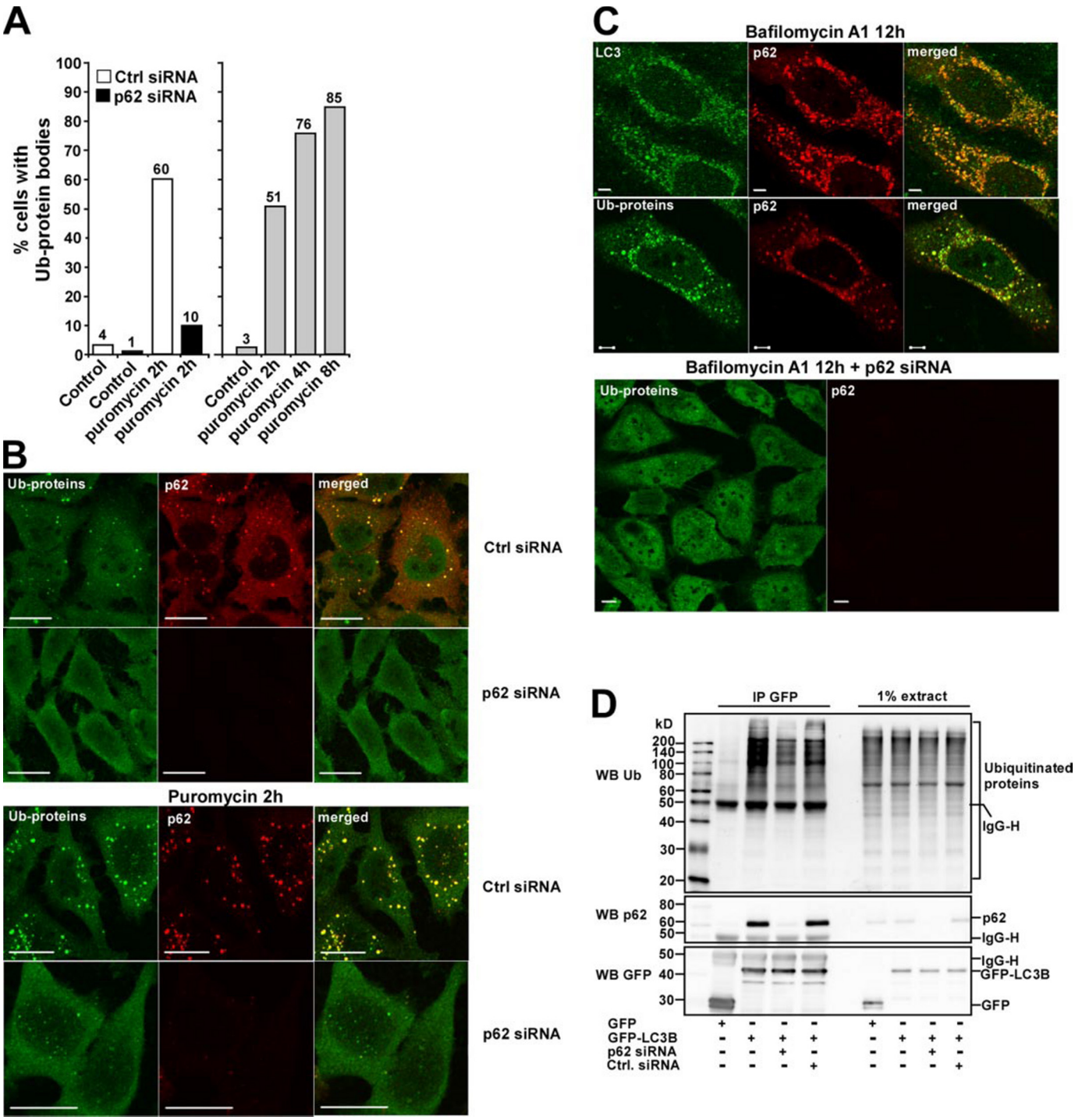

FIGURE 9. **ALIS are indistinguishable from p62 inclusion bodies and dependent on p62 for their formation.** *A* and *B,* formation of cytoplasmic polyubiquitin-positive bodies (ALIS) is dependent on p62. HeLa cells were transfected with control (*Ctrl*) siRNA or p62 siRNA as indicated. Cell cultures were stressed with puromycin (5 μg/ml) as indicated to induce formation of ALIS and then fixed and stained with p62 Ab and FK2 mAb. *A,* number of cells containing ubiquitinated (*Ub*) protein bodies increased with time after addition of puromycin reaching a maximum after 8 h (*right panel*). The induction of ubiquitinated protein bodies (aggregates) following puromycin treatment or amino acid starvation is strongly inhibited by siRNA-mediated depletion of p62 (*left panel*). Results from representative experiments are shown. From 300 to 600 cells were scored for the presence or absence of FK2-positive round bodies for each data point shown (each *bar*). Only cells that did not stain positive for p62 following transfection with p62 siRNA were included in these quantitations. *B,* representative confocal images of cells from experiments used to perform the quantitations shown in *A*. Note that knockdown of p62 results in loss of FK2 staining in cytoplasmic bodies. *C,* p62 links ubiquitinated proteins to LC3 in cytoplasmic bodies that become degraded by autophagy. Endogenous LC3, ubiquitinated proteins, and p62 co-localize in autolysosomes in bafilomycin A_1-treated cells (*upper panels*). Depletion of p62 blocks the recruitment of ubiquitinated proteins to autolysosomes (*lower panel*). HeLa cells were incubated with bafilomycin A_1 (0.2 μM) for 12 h, fixed, and immunostained with LC3 mAb, FK2 mAb, and p62 Ab. *D,* siRNA-mediated knockdown of p62 reduces the interaction of transiently expressed GFP-LC3B with ubiquitinated proteins. GFP or GFP-LC3B was immunoprecipitated from total cellular extracts of HeLa cells that had been treated with siRNA to p62 or control siRNA. Co-purified ubiquitinated proteins were detected using the FK2 mAb. *Scale bars*: 5 μm in *B* and *C, upper panels*, and 10 μm in *C, lower panel*. *WB*, Western blot.

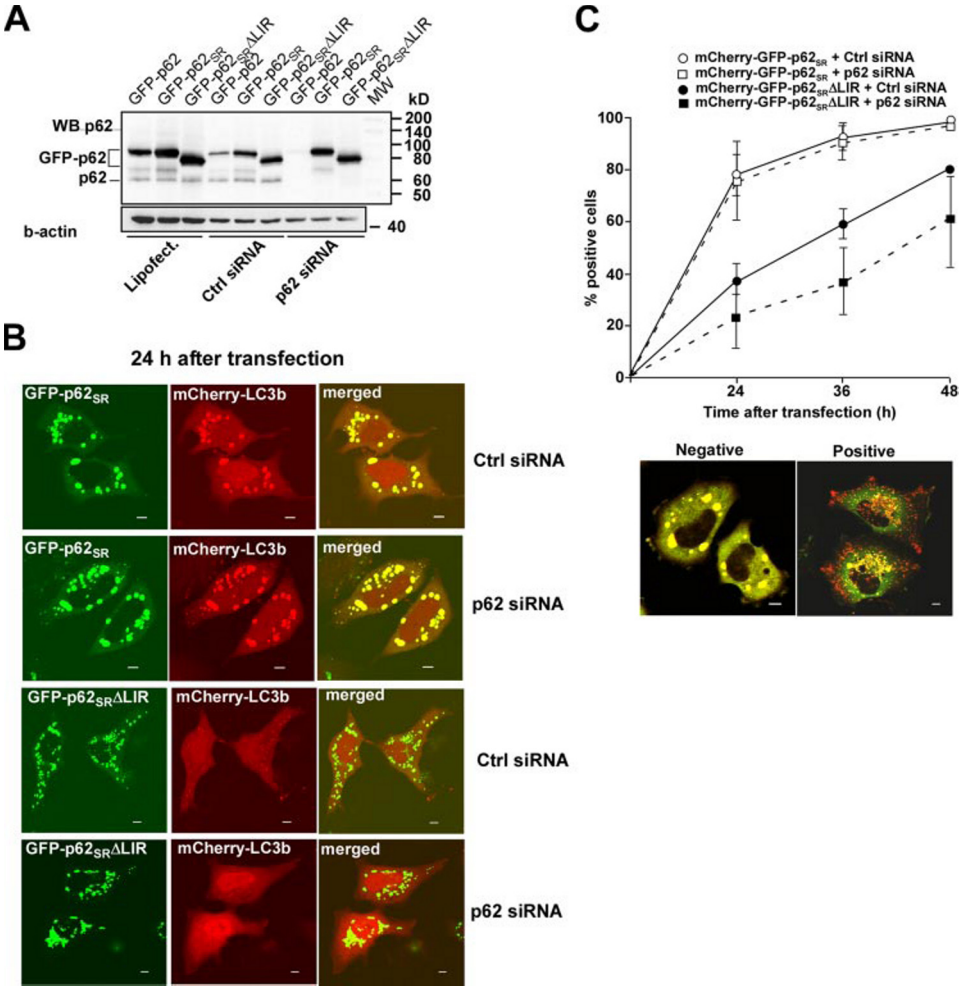

FIGURE 10. **The LIR of p62 is required for autophagic degradation of p62 bodies.** *A,* efficient knockdown of wild-type p62 fused to GFP and endogenous p62 following transfection with siRNA *versus* p62. The siRNA-resistant mutant (*SR*) of p62 fused to GFP was unaffected. Total cell lysates of HeLa cells transiently transfected with the indicated expression constructs and siRNAs were subjected to SDS-PAGE and immunoblotted with anti-p62 (*upper panel*) or anti-actin (*lower panel*) antibodies. *WB*, Western blot; *Ctrl,* control. *B,* p62Δ LIR cannot recruit LC3B to p62-positive inclusion bodies. HeLa cells were transiently transfected with the indicated constructs and siRNAs and imaged 24 h after transfection. *C,* LIR of p62 is important for targeting of p62 to acidic autophagic vesicles (amphisomes and autolysosomes). HeLa cells were transiently transfected with the indicated constructs of p62 and siRNAs. 24, 36, and 48 h after transfection cells containing red vesicles with a diameter of 0.5–1 μm were counted and presented as a percentage of total cells counted (*upper panel*). Representative images of cells were counted as negative or positive for localization of p62 to autophagic vesicles (*lower panel*). *Scale bars* are 5 μm.

p62 Is Required for Constitutive Autophagic Degradation of Ubiquitinated Proteins—Staining of bafilomycin A_1-treated HeLa cells with the FK2 monoclonal antibody, which recognizes mono- and polyubiquitin covalently attached to proteins (46), revealed that ubiquitinated proteins are present in autophagic vesicles, together with LC3 and p62 (Fig. 9*C*). As expected, depletion of p62 reduced, but did not prevent, accumulation of LC3 in autophagic vesicles following treatment with bafilomycin A_1 (data not shown). However, we observed a dramatic reduction in the amount of ubiquitinated proteins within autolysosomes in cells following siRNA-mediated knockdown of p62 (Fig. 9*C*). This strongly supports the notion that p62 has an essential role in the autophagic degradation of inclusions containing ubiquitinated proteins.

In p62 bodies, polyubiquitinated proteins co-localize with LC3. As an alternative to experiments with immunostaining of cells, we immunoprecipitated GFP-LC3B expressed in HeLa cells and looked for co-immunoprecipitation of ubiquitinated proteins. As shown in Fig. 9*D*, substantial amounts of ubiquitinated proteins were co-immunoprecipitated with GFP-LC3B. However, when p62 protein levels were severely reduced following transfection with siRNA against p62, there was a significant reduction in the amount of co-immunoprecipitated ubiquitinated proteins. This is entirely consistent with the results obtained by immunostaining of cells following siRNA-mediated knockdown of p62.

The LIR of p62 Is Required for the Autophagic Degradation of p62 Bodies—p62 can polymerize via its PB1 domain, and overexpression of mutant constructs of p62 will result in formation of polymeric structures containing both endogenous wild-type and overexpressed mutant forms of the protein. To overcome this problem and enable transient expression of p62 mutants in cells depleted of endogenous p62, we introduced silent mutations in two codons of p62 in the middle of the target sequence for siRNA 2 (see "Experimental Procedures"). As is evident from the immunoblot in Fig. 10*A*, these mutations rendered transiently expressed GFP-p62 constructs resistant to the siRNA, whereas expression of wild-type GFP-p62 was efficiently inhibited. To test if LIR is needed for the recruitment of LC3B into p62 bodies, siRNA-resistant GFP-p62 (GFP-$p62_{SR}$) or siRNA-resistant GFP-p62 with LIR deleted (GFP-$p62_{SR}$ΔLIR) was expressed in HeLa cells together with mCherry-LC3B and siRNA toward p62 or scrambled control siRNA. Representative images of cells containing large p62 inclusion bodies are shown in Fig. 10*B*. As expected, virtually every inclusion body formed by GFP-$p62_{SR}$ contained a large amount of mCherry-LC3B, both in the presence and absence of p62 siRNA. Strikingly, mCherry-LC3B was completely diffusely localized in cells transfected with GFP-$p62_{SR}$ΔLIR and p62 siRNA. In the presence of endogenous p62, there was some recruitment of mCherry-LC3B into GFP-$p62_{SR}$ΔLIR bodies, but this was severely reduced compared with the p62 construct containing the LIR (Fig. 10*B*). These results demonstrate that LIR is required for recruitment of LC3B into p62 bodies.

We then addressed the question whether LIR is important for the autophagic degradation of p62. In these experiments,

mCherry-GFP-p62$_{SR}$ or mCherry-GFP-p62$_{SR}$ΔLIR was expressed in HeLa cells together with siRNAs. For each experiment, we counted the fraction of cells that contained p62 in acidic vesicles. Cells with more than five acidic p62 dots were counted as positive (Fig. 10*C*). As expected, most cells expressing mCherry-GFP-p62$_{SR}$ recruited the protein into acidic vesicles, whereas deletion of LIR strongly reduced the ability of p62 to be recruited into acidic vesicles, both when co-expressed with siRNA toward p62 or scrambled control siRNA (Fig. 10*C*). This fits well with the observation above that LC3B was poorly recruited into p62 bodies formed by p62$_{SR}$ΔLIR, even in cells expressing a normal level of endogenous p62 (Fig. 10*B*). However, it should be noted that at 48 h after transfection p62$_{SR}$ΔLIR also became gradually recruited into autophagosomes. Because siRNA depletion of p62 is not complete, we attribute that effect to residual endogenous p62 that helps recruit LC3 into structures containing p62$_{SR}$ΔLIR. In conclusion, our results suggest that recruitment of LC3 via the LIR of p62 is essential for autophagic degradation of p62 and p62-positive bodies.

DISCUSSION

In this study we show that p62 binds directly to LC3A and -B and other human Atg8 homologues such as GABARAP, GABARAPL1, and GABARAPL2. In fact, p62 is likely the major LC3-interacting protein in HeLa cells (Fig. 1*A*). The interaction between p62 and Atg8 homologues is mediated by a 22-amino acid acidic peptide motif (LIR) in p62 and requires both the N- and C-terminal subdomains of LC3B. Interestingly, one recent large scale yeast two-hybrid screen suggested an interaction between p62 and LC3B (47) and another an interaction between p62 and GABARAPL1 and -2 (48). We use a novel double tag strategy to demonstrate that the interaction between p62 and LC3 is necessary for degradation of p62-positive bodies containing polyubiquitinated proteins, by autophagy. By binding polyubiquitinated proteins via the UBA domain, polymerizing via its PB1 domain, and binding to LC3 via the LIR motif, p62 forms protein bodies containing LC3 that are degraded by autophagy.

LC3 belongs to the family of microtubule-associated proteins (MAPs) and is known to interact with both MAP1A and -B. MAP1B binds to both LC3-I and -II, and overexpression of MAP1B results in reduced levels of LC3-II and reduced numbers of GFP-LC3-labeled autophagosomes (49). Interestingly, we identified MAP1B by mass spectrometry as a prominent band co-immunoprecipitating with GFP-LC3 from a HeLa cell lysate (Fig. 1*A*).

GFP-LC3 has been used extensively as a marker for autophagy (7, 37). However, because GFP-LC3 is also recruited to inclusions, the use of this marker may not always give reliable information about the autophagic process. The pH lability of GFP makes it impossible to follow GFP-LC3 after the short lived autophagosomes fuse with lysosomes. Fusion with late endosomes to create amphisomes may also lead to an environment where the fluorescence from GFP is quenched due to low pH. We therefore fused LC3 to the acid-stable fluorescent protein mCherry, and mCherry-LC3 could easily be followed into amphisomes and autolysosomes. By combining these two tags, in mCherry-GFP-LC3 and mCherry-GFP-p62, we were able to distinguish inclusions and autophagosomes (green and red) from amphisomes/autolysosomes (red only). Use of AlexaFluor 647 dextran and LAMP1 antibodies confirmed that the red fluorescence of mCherry remains intact, whereas virtually all GFP fluorescence is lost in amphisomes and autolysosomes. The double tag can be used for live cell imaging and is strikingly informative about the autophagic process. When used to study p62 bodies, green GFP-positive structures constitute p62 inclusions and autophagosomes, whereas bodies that are red only represent acidic amphisomes/autolysosomes. The double tag approach is not limited to autophagic proteins such as LC3 and p62. The tag should therefore serve as a valuable tool to study internalization and lysosomal degradation of plasma membrane receptors by live cell imaging.

Because p62 itself is degraded by autophagy, both we and others have found a general correlation between inhibition of autophagy and increased levels of p62 (16, 29, 49). Clearly, p62 may also be used as an autophagic marker. p62 has a less diffuse localization pattern than LC3, making it easier to identify the small autophagic vesicles using this marker. However, it is important to keep in mind that by transiently overexpressing p62, the formation of inclusion bodies is also increased.

Using fusion proteins containing the mCherry-GFP tandem tag, we demonstrate that cytoplasmic bodies containing p62, LC3, and ubiquitinated proteins are degraded by autophagy. Both large (more than 1 μm in diameter) and small (less than 0.5 μm in diameter) protein bodies could be engulfed by autophagy. Small p62 bodies changed from neutral (yellow) to acidic (red) within a minute, whereas larger structures needed considerably more time to become acidified. However, we observed an accumulation of p62 in autophagic structures also in cells that did not contain large p62 bodies. Our current hypothesis is that p62 bodies are degraded by basal constitutive autophagy even before they grow to sizes detectable by light microscopy but that also large structures are degraded. In Atg5$^{-/-}$ MEFs, which are completely deficient in autophagy (44, 45), the acidic p62-containing vesicles were absent. Using Atg5$^{-/-}$ MEFs with inducible expression of an Atg5 minigene (cDNA), we could show that mCherry-GFP-p62 could enter the autophagic pathway when Atg5 was expressed. Our results suggest the following: (i) p62 plays an architectural role in the formation of inclusion bodies and (ii) p62 also links these structures to the autophagic machinery via direct interaction with LC3s and/or other mammalian Atg8 homologues. The p62 LC3 interacting region, LIR, was found indispensable for LC3 recruitment into p62-positive inclusion bodies. Our studies with purified recombinant proteins show that p62 binds to both the pro-form and the processed form I of LC3 (Fig. 1 and data not shown). Presumably the isolation membrane is recruited to p62-positive bodies concomitant with or following lipidation of LC3. It will be important to identify proteins that recognize LC3 or p62 (or both) and simultaneously are bound to the forming isolation membrane, either directly or indirectly.

Our data clearly show that puromycin-induced ALIS and p62-positive inclusion bodies are the same structures and that their formation depends on the presence of p62. In fact, similar

bodies can also be induced by overexpression of p62 or proteasomal inhibition. The latter very efficiently induces p62 bodies (29).

Mutations in the p62/SQSTM1 gene at 5q35 are a common cause of classical, adult onset Paget disease of the bone. Between 30 and 50% of the familial cases are due to dominant acting mutations leading to loss of function of polyubiquitin binding by either deletion of the UBA domain or point mutations within this domain (27, 50). Genetic inactivation of p62 in mice leads to impaired osteoclastogenesis and mature onset obesity with insulin resistance (51, 52). It will be important to elucidate how the role p62 has in protein degradation by autophagy is connected to the complex phenotypic consequences observed upon knocking out p62. Atg5$^{-/-}$ or Atg7$^{-/-}$ mice die soon after birth, whereas the p62 knock-out mice show no extensive lethality at this stage. p62 is clearly a stress-induced protein increasing after oxygen radical stress, inhibition of proteasomal activity (53), and in response to expression of mutant Huntingtin (23). Hence, p62 may make an important contribution to autophagy under conditions of oxidative stress and in the aging organism. It will be interesting to learn if p62 knock-out mice show a late onset neurodegenerative phenotype. Genetic models of neurodegenerative diseases where aggregation-prone mutant proteins are expressed in a p62-deficient background will clearly also yield important insights.

Acknowledgments—We are very grateful to Noboru Mizushima for the generous gift of MEF cell lines. We are also indebted to R. Tsien for the kind gift of pRSET-B-mCherry and H. Berglund for pDEST-TH1. We acknowledge Anne Simonsen for help with MEF cells. We are grateful to Harald Stenmark for the gift of polyclonal mCherry antibody and for critical reading of the manuscript.

REFERENCES

1. Goldberg, A. L. (2003) *Nature* **426,** 895–899
2. Cuervo, A. M. (2004) *Trends Cell Biol.* **14,** 70–77
3. Klionsky, D. J. (2005) *J. Cell Sci.* **118,** 7–18
4. Yoshimori, T. (2004) *Biochem. Biophys. Res. Commun.* **313,** 453–458
5. Eskelinen, E. L. (2005) *Autophagy* **1,** 1–10
6. Ohsumi, Y. (2001) *Nat. Rev. Mol. Cell Biol.* **2,** 211–216
7. Kabeya, Y., Mizushima, N., Yamamoto, A., Oshitani-Okamoto, S., Ohsumi, Y., and Yoshimori, T. (2004) *J. Cell Sci.* **117,** 2805–2812
8. Tanida, I., Ueno, T., and Kominami, E. (2004) *J. Biol. Chem.* **279,** 47704–47710
9. Sou, Y. S., Tanida, I., Komatsu, M., Ueno, T., and Kominami, E. (2006) *J. Biol. Chem.* **281,** 3017–3024
10. He, H., Dang, Y., Dai, F., Guo, Z., Wu, J., She, X., Pei, Y., Chen, Y., Ling, W., Wu, C., Zhao, S., Liu, J. O., and Yu, L. (2003) *J. Biol. Chem.* **278,** 29278–29287
11. Xin, Y., Yu, L., Chen, Z., Zheng, L., Fu, Q., Jiang, J., Zhang, P., Gong, R., and Zhao, S. (2001) *Genomics* **74,** 408–413
12. Nixon, R. A. (2006) *Trends Neurosci.* **29,** 528–535
13. Hara, T., Nakamura, K., Matsui, M., Yamamoto, A., Nakahara, Y., Suzuki-Migishima, R., Yokoyama, M., Mishima, K., Saito, I., Okano, H., and Mizushima, N. (2006) *Nature* **441,** 885–889
14. Komatsu, M., Waguri, S., Chiba, T., Murata, S., Iwata, J., Tanida, I., Ueno, T., Koike, M., Uchiyama, Y., Kominami, E., and Tanaka, K. (2006) *Nature* **441,** 880–884
15. Komatsu, M., Waguri, S., Ueno, T., Iwata, J., Murata, S., Tanida, I., Ezaki, J., Mizushima, N., Ohsumi, Y., Uchiyama, Y., Kominami, E., Tanaka, K., and Chiba, T. (2005) *J. Cell Biol.* **169,** 425–434
16. Mizushima, N., and Hara, T. (2006) *Autophagy* **2,** 302–304
17. Szeto, J., Kaniuk, N. A., Canadien, V., Nisman, R., Mizushima, N., Yoshimori, T., Bazett-Jones, D. P., and Brumell, J. H. (2006) *Autophagy* **2,** 189–199
18. Lelouard, H., Gatti, E., Cappello, F., Gresser, O., Camosseto, V., and Pierre, P. (2002) *Nature* **417,** 177–182
19. Lelouard, H., Ferrand, V., Marguet, D., Bania, J., Camosseto, V., David, A., Gatti, E., and Pierre, P. (2004) *J. Cell Biol.* **164,** 667–675
20. Kopito, R. R. (2000) *Trends Cell Biol.* **10,** 524–530
21. Kuusisto, E., Salminen, A., and Alafuzoff, I. (2001) *Neuroreport* **12,** 2085–2090
22. Kuusisto, E., Salminen, A., and Alafuzoff, I. (2002) *Neuropathol. Appl. Neurobiol.* **28,** 228–237
23. Nagaoka, U., Kim, K., Jana, N. R., Doi, H., Maruyama, M., Mitsui, K., Oyama, F., and Nukina, N. (2004) *J. Neurochem.* **91,** 57–68
24. Zatloukal, K., Stumptner, C., Fuchsbichler, A., Heid, H., Schnoelzer, M., Kenner, L., Kleinert, R., Prinz, M., Aguzzi, A., and Denk, H. (2002) *Am. J. Pathol.* **160,** 255–263
25. Lamark, T., Perander, M., Outzen, H., Kristiansen, K., Øvervatn, A., Michaelsen, E., Bjørkøy, G., and Johansen, T. (2003) *J. Biol. Chem.* **278,** 34568–34581
26. Wilson, M. I., Gill, D. J., Perisic, O., Quinn, M. T., and Williams, R. L. (2003) *Mol. Cell* **12,** 39–50
27. Cavey, J. R., Ralston, S. H., Hocking, L. J., Sheppard, P. W., Ciani, B., Searle, M. S., and Layfield, R. (2005) *J. Bone Miner. Res.* **20,** 619–624
28. Vadlamudi, R. K., Joung, I., Strominger, J. L., and Shin, J. (1996) *J. Biol. Chem.* **271,** 20235–20237
29. Bjørkøy, G., Lamark, T., Brech, A., Outzen, H., Perander, M., Øvervatn, A., Stenmark, H., and Johansen, T. (2005) *J. Cell Biol.* **171,** 603–614
30. Shevchenko, A., Wilm, M., Vorm, O., and Mann, M. (1996) *Anal. Chem.* **68,** 850–858
31. Peters, P. J., Neefjes, J. J., Oorschot, V., Ploegh, H. L., and Geuze, H. J. (1991) *Nature* **349,** 669–676
32. Slot, J. W., Geuze, H. J., Gigengack, S., Lienhard, G. E., and James, D. E. (1991) *J. Cell Biol.* **113,** 123–135
33. Kouno, T., Mizuguchi, M., Tanida, I., Ueno, T., Kanematsu, T., Mori, Y., Shinoda, H., Hirata, M., Kominami, E., and Kawano, K. (2005) *J. Biol. Chem.* **280,** 24610–24617
34. Sugawara, K., Suzuki, N. N., Fujioka, Y., Mizushima, N., Ohsumi, Y., and Inagaki, F. (2004) *Genes Cells* **9,** 611–618
35. Tanida, I., Ueno, T., and Kominami, E. (2004) *Int. J. Biochem. Cell Biol.* **36,** 2503–2518
36. Kabeya, Y., Mizushima, N., Ueno, T., Yamamoto, A., Kirisako, T., Noda, T., Kominami, E., Ohsumi, Y., and Yoshimori, T. (2000) *EMBO J.* **19,** 5720–5728
37. Mizushima, N. (2004) *Int. J. Biochem. Cell Biol.* **36,** 2491–2502
38. Shaner, N. C., Steinbach, P. A., and Tsien, R. Y. (2005) *Nat. Meth.* **2,** 905–909
39. Kielian, M. C., and Cohn, Z. A. (1982) *J. Cell Biol.* **93,** 875–882
40. Zen, K., Biwersi, J., Periasamy, N., and Verkman, A. S. (1992) *J. Cell Biol.* **119,** 99–110
41. Shaner, N. C., Campbell, R. E., Steinbach, P. A., Giepmans, B. N., Palmer, A. E., and Tsien, R. Y. (2004) *Nat. Biotechnol.* **22,** 1567–1572
42. Fass, E., Shvets, E., Degani, I., Hirschberg, K., and Elazar, Z. (2006) *J. Biol. Chem.* **281,** 36303–36316
43. Escola, J. M., Kleijmeer, M. J., Stoorvogel, W., Griffith, J. M., Yoshie, O., and Geuze, H. J. (1998) *J. Biol. Chem.* **273,** 20121–20127
44. Hosokawa, N., Hara, Y., and Mizushima, N. (2006) *FEBS Lett.* **580,** 2623–2629
45. Kuma, A., Hatano, M., Matsui, M., Yamamoto, A., Nakaya, H., Yoshimori, T., Ohsumi, Y., Tokuhisa, T., and Mizushima, N. (2004) *Nature* **432,** 1032–1036
46. Fujimuro, M., Sawada, H., and Yokosawa, H. (1994) *FEBS Lett.* **349,** 173–180
47. Stelzl, U., Worm, U., Lalowski, M., Haenig, C., Brembeck, F. H., Goehler, H., Stroedicke, M., Zenkner, M., Schoenherr, A., Koeppen, S., Timm, J., Mintzlaff, S., Abraham, C., Bock, N., Kietzmann, S., Goedde, A., Toksoz, E., Droege, A., Krobitsch, S., Korn, B., Birchmeier, W., Lehrach, H., and Wanker, E. E. (2005) *Cell* **122,** 957–968

48. Rual, J. F., Venkatesan, K., Hao, T., Hirozane-Kishikawa, T., Dricot, A., Li, N., Berriz, G. F., Gibbons, F. D., Dreze, M., Ayivi-Guedehoussou, N., Klitgord, N., Simon, C., Boxem, M., Milstein, S., Rosenberg, J., Goldberg, D. S., Zhang, L. V., Wong, S. L., Franklin, G., Li, S., Albala, J. S., Lim, J., Fraughton, C., Llamosas, E., Cevik, S., Bex, C., Lamesch, P., Sikorski, R. S., Vandenhaute, J., Zoghbi, H. Y., Smolyar, A., Bosak, S., Sequerra, R., Doucette-Stamm, L., Cusick, M. E., Hill, D. E., Roth, F. P., and Vidal, M. (2005) *Nature* **437,** 1173–1178
49. Wang, Q. J., Ding, Y., Kohtz, D. S., Mizushima, N., Cristea, I. M., Rout, M. P., Chait, B. T., Zhong, Y., Heintz, N., and Yue, Z. (2006) *J. Neurosci.* **26,** 8057–8068
50. Daroszewska, A., and Ralston, S. H. (2006) *Nat. Clin. Pract. Rheumatol.* **2,** 270–277
51. Duran, A., Serrano, M., Leitges, M., Flores, J. M., Picard, S., Brown, J. P., Moscat, J., and Diaz-Meco, M. T. (2004) *Dev. Cell* **6,** 303–309
52. Rodriguez, A., Duran, A., Selloum, M., Champy, M. F., Diez-Guerra, F. J., Flores, J. M., Serrano, M., Auwerx, J., Diaz-Meco, M. T., and Moscat, J. (2006) *Cell Metab.* **3,** 211–222
53. Ishii, T., Yanagawa, T., Yuki, K., Kawane, T., Yoshida, H., and Bannai, S. (1997) *Biochem. Biophys. Res. Commun.* **232,** 33–37
54. Hammarstrom, M., Hellgren, N., van Den Berg, S., Berglund, H., and Hard, T. (2002) *Protein Sci.* **11,** 313–321
55. Simonsen, A., Birkeland, H. C., Gillooly, D. J., Mizushima, N., Kuma, A., Yoshimori, T., Slagsvold, T., Brech, A., and Stenmark, H. (2004) *J. Cell Sci.* **117,** 4239–4251